Nuclear Science and Techniques (2023) 34:152
https://doi.org/10.1007/s41365-023-01308-x

Predictions of nuclear charge radii based on the convolutional neural network

Ying-Yu Cao[1] · Jian-You Guo[2] · Bo Zhou[1,3]

Received: 19 May 2023 / Revised: 3 August 2023 / Accepted: 5 August 2023 / Published online: 26 October 2023

Abstract
In this study, we developed a neural network that incorporates a fully connected layer with a convolutional layer to predict the nuclear charge radii based on the relationships between four local nuclear charge radii. The convolutional neural network (CNN) combines the isospin and pairing effects to describe the charge radii of nuclei with $A \geq 39$ and $Z \geq 20$. The developed neural network achieved a root mean square (RMS) deviation of 0.0195 fm for a dataset with 928 nuclei. Specifically, the CNN reproduced the trend of the inverted parabolic behavior and odd–even staggering observed in the calcium isotopic chain, demonstrating reliable predictive capability.

Keywords Nuclear charge radii · Machine learning · Neural network

1 Introduction

Nuclear charge radius is a fundamental property of the nucleus, along with its mass, density, spin, and moments [1–3]. This reveals vital information regarding the nuclear structure, such as shell closure, halo effect, and electromagnetic properties [4–6]. To date, various experimental techniques have been employed to measure the nuclear radius, including the scattering of high-energy particles in the nucleus [7], atomic spectroscopy [8, 9], X-ray spectroscopy excited by μ atoms [10, 11], and isotopic shifts in the ultrafine structure of the atomic spectra [12]. The CR2013 database contains the root mean square (RMS) nuclear charge radii for 909 isotopes of 92 elements, from hydrogen to curium [13], with neutron numbers ranging from 0 to 152. More recently, the measurement of charge radii have been extended to nuclei much beyond the β-stability line. The latest CR2021 database includes data for 129 charge radii of nuclei, with $A \geq 21$ and $Z \geq 14$ [14].

Numerous theoretical methods have been developed to describe and predict charge radii, which can be broadly classified into three major categories: macroscopic, microscopic, and traditionally macroscopic. Microscopic models are based on effective and real interactions to study the structure and properties of nuclei. Microscopic models include the Hartree–Fock–Bogoliubov (HFB) model, relativistic mean-field (RMF) theory, *ab initio* calculations, and the cluster model [15–19]. For instance, the HFB21 model achieved a high level of accuracy for predicting the charge radii, with an RMS deviation of 0.027 fm for 782 measured charge radii [16]. Traditional macroscopic models rely on phenomenological laws to describe charge radii [20–22], including the $A^{1/3}$ and $Z^{1/3}$ laws [23–25], where A represents the mass number and Z denotes the number of protons. In addition, the nuclear charge radii can be accurately predicted using the Garvey–Kelson relationship. As such, these relationships describe the nuclear charge radii based on the relative position of a given nucleus with respect to other known charge radii [26–28]. Although phenomenological models can accurately describe the global trends in nuclear charge radii, they often struggle to reveal the underlying physical quantities within the individual nucleus.

This work was supported by Shanghai "Science and Technology Innovation Action Plan" Project (No. 21ZR140950).

✉ Bo Zhou
zhou_bo@fudan.edu.cn

[1] Key Laboratory of Nuclear Physics and Ion-beam Application (MOE), Institute of Modern Physics, Fudan University, Shanghai 200433, China

[2] School of Physics and Optoelectronics Engineering, Anhui University, Hefei 230601, China

[3] Shanghai Research Center for Theoretical Nuclear Physics, NSFC and Fudan University, Shanghai 200438, China

Machine learning is widely applied in physics owing to the availability of large datasets and powerful hardware technologies. It has proved to be highly effective in processing complex data, uncovering hidden patterns, and solving stochastic processes. In fields such as high-energy physics and astrophysics that requires processing enormous amounts of data [29–32], machine learning is essential for analyzing the evolution and morphology of galaxies [33–35] and extracting information from high-energy reactions [36–39]. In nuclear physics, machine learning techniques such as artificial neural networks (ANNs) [40, 41], Bayesian neural networks (BNNs) [42–45], and radial basis functions (RBFs) have been used to improve the accuracy of predictions of nuclear properties such as nuclear mass [46–49], charge radius [50, 51], and β-decay half-lives [52]. Furthermore, convolutional neural networks (CNNs) have been used to solve problems pertaining to density functional theory [53, 54]. Currently, fully connected neural networks are generally employed to describe the properties of nuclei in nuclear physics, with several weights and high computational complexities. To mitigate this complexity, we considered a CNN with local connections and weight sharing.

In this paper, we present a novel approach for improving the prediction of nuclear charge radii within local charge radius (CR) relations by utilizing a CNN. In Sect. 2, we provide a brief overview of the theoretical background of local CR relations and the principles of CNN. In Sect. 3, we describe the proposed methodology for training a CNN using existing experimental data on nuclear radii. We present the results of our analysis, including the global RMS deviation obtained by the proposed model, and provide relevant discussions and predictions based on the findings. Finally, the present findings and the conclusions of this study are summarized, highlighting the potential of CNN as powerful tools for improving the prediction of nuclear charge radii.

2 Theoretical formalism

The Garvey–Kelson relationship was introduced in 1966 as a method for predicting the mass of nuclei. Owing to the complexity of the Hamiltonian for a multibody system, the mass of a nucleus cannot be directly calculated from the first principles. Instead, the mass of a given nucleus can be accurately inferred from the masses of its neighboring nuclei [55, 56]. Similarly, four local CR relations were proposed [27], which are based on the charge radii of the four neighboring nuclei and are referred to as the 1n − 1p, 1n − 2p, 2n − 1p, and 2n − 2p CR relations, respectively.

$$\begin{aligned}\delta R_{in-jp} =& 0, \quad i,j = 1,2,\\ \delta R_{in-jp} =& R(N,Z) + R(N-i,Z-j)\\ &- R(N-i,Z) - R(N,Z-j).\end{aligned} \tag{1}$$

As reported in Ref. [27], the RMS deviation was 0.0078 fm for all nuclei with $N, Z \geq 2$. However, the Garvey–Kelson relationships are expressed as local formulas. The radii of the neighboring nuclei must be known to obtain the radius of a specific nucleus. Inspired by Refs. [27, 28], we aimed to utilize local CR relationships to characterize the global nuclear radius.

When $i = 1$ and $j = 1$, δR_{1n-1p} represents the charge radii relationship between the four nearest neighbor nuclei, and the following four subrelations can be derived similarly:

$$\begin{aligned}\delta R_{1n-1p} =& R(N,Z) + R(N-1,Z-1)\\ &- R(N-1,Z) - R(N,Z-1),\end{aligned} \tag{2}$$

$$\begin{aligned}\delta R_{1n-1p} =& R(N+1,Z+1) + R(N,Z)\\ &- R(N,Z+1) - R(N+1,Z),\end{aligned} \tag{3}$$

$$\begin{aligned}\delta R_{1n-1p} =& R(N+1,Z) + R(N,Z-1)\\ &- R(N,Z) - R(N+1,Z-1),\end{aligned} \tag{4}$$

$$\begin{aligned}\delta R_{1n-1p} =& R(N,Z+1) + R(N-1,Z)\\ &- R(N-1,Z+1) - R(N,Z).\end{aligned} \tag{5}$$

Therefore, for $i, j = 1, 2$, we can utilize 16 subrelations to calculate $R(N, Z)$. Subsequently, these 16 subrelations are added to obtain a radius relation for the 25 nuclei, and 25 nuclear charge radii were reshaped into a 5×5 matrix with the corresponding coefficients. This local relationship is displayed in Fig. 1a. Similarly, we considered the local relation of the nine nuclear charge radii, as depicted in Fig. 1b.

CNNs are commonly applied in the field of computer vision [57]. They can identify local features in images using fewer parameters and effectively reduce overfitting. By arranging the charge radii from CR2013 for nuclei with $Z \geq 18$ (Fig. 1), a 79×153 nuclear charge radius matrix was formed. The coefficient matrix in Fig. 1 is treated as a convolutional kernel in CNNs. The sliding of the convolutional kernel across the matrix forms a convolution process that is crucial for CNNs. The two-dimensional convolution formula is stated as follows:

$$O(u,v) = \sum_i \sum_j g(i,j)h(u-i,v-j), \tag{6}$$

where $O(u, v)$ denotes the value of the element at coordinates (u, v) in the output matrix and $g(i, j)$ denotes the value of the element at coordinates (i, j) in the input matrix.

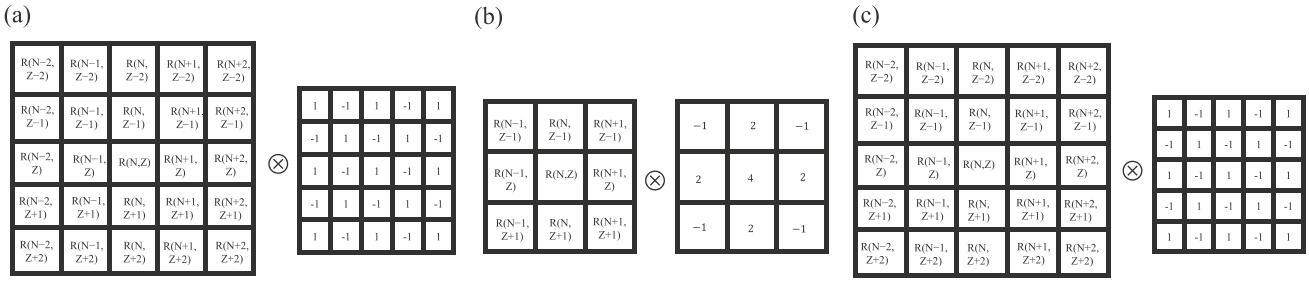

Fig. 1 (Color online) **a** Radii relations between 25 neighboring nuclei, visualized as a matrix formed by rearranging the 25 nuclei and convolving it with the coefficient matrix. **b** Radii relations between 9 neighboring nuclei. **c** Odd–even staggering effect across 25 nuclei

Similarly, $h(u-i, v-j)$ represents the value of the element at the coordinates $(u-i, v-j)$ in the convolution kernel.

The empirical formula developed by Angeli et al. [23, 58]:

$$R_c(Z,N,A) = r_0\left[1 - a\left(\frac{N-Z}{A}\right) + \frac{b}{A}\right]A^{1/3}, \tag{7}$$

where $r_0 = 0.9561$ fm, $a = 0.1426$, and $b = 2.1057$. This three-parameter formula improves the description of the radius of even–even nuclei, and the RMS deviation (the root mean square difference between calculated nuclear charge radii and the experimental values) is 0.0385 fm for nuclei with $A \geq 39$ and $Z \geq 20$, which were used as the training set. Thus, odd–even staggering crucially affects several isotopes. Therefore, by introducing a δ term into Eq. (7), we can obtain:

$$R_c(Z,N,A) = r_0\left[1 - a\left(\frac{N-Z}{A}\right) + \frac{b}{A} + \frac{c\delta}{A}\right]A^{1/3}, \tag{8}$$

where r_0 =0.9562 fm, $a = 0.1429$, $b = 2.0825$, and $c = 0.0694$. The parameters were obtained by fitting the training set and the RMS deviation was 0.0385 fm. Similarly, we constructed a pairing term for δ local relations to describe the odd–even staggering effect of the charge radius for the nuclei portrayed in Fig. 1c. Considering the characteristics of the nuclei near the β-stability line, we added the isospin dependence T, which is also referred to as the NP relation [45]. δ and T, defined as follows:

$$\begin{aligned} \delta &= \frac{(-1)^Z + (-1)^N}{2}, \\ T &= \frac{N-Z}{A}. \end{aligned} \tag{9}$$

The structure of the neural network is depicted in Fig. 2. The neural network comprised an input layer, a fully connected layer, a convolutional layer, and two output layers. The input data are the proton number Z, neutron number N, and mass number A of 928 nuclei. The activation function from the input layer to the fully connected layer is Mish(x), and its formula is expressed as follows:

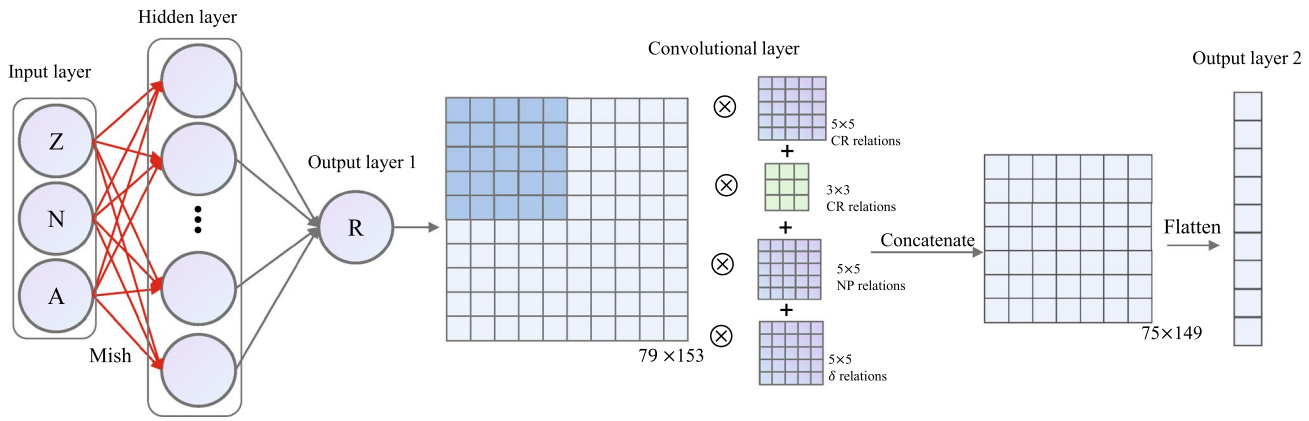

Fig. 2 (Color online) Neural network structure used herein. Input data comprises proton number Z, mass number A, and neutron number N. Neural network has two hidden layers with eight and four neurons, respectively. The hidden layer processes the data to output numerous nuclear charge radii. The data were reshaped into a matrix and fed into the convolutional layer for further processing. After the convolutional layer has processed the data, the final output was obtained. The stride was 1 for the convolutional layer

$$\mathrm{Mish}(x) = x \cdot \tanh(\ln(1 + \mathrm{e}^{x})), \tag{10}$$

denotes the output of a fully connected layer. These three layers formed a fully connected (FC) net. We obtained a CR matrix with 79 rows and 153 columns using FC net. We then considered the CR matrix as the input to the convolutional layer. As depicted in Fig. 2, the convolutional layer comprises four components: convolution of the nuclear radius matrix with 5×5, 3×3 CR relations, 5×5 isospin dependence (NP relations), and 5×5 delta relations. Thereafter, we assigned each component a weight w_i and added it to the final output of the neural networks. The calculation process for the convolutional layer can be expressed as

$$f(O) = \sum_{i}^{4} R(\omega_i O_i) + b, \tag{11}$$

where $R(x)$ represents the activation function and O_i represents the convolutional result, as depicted in Eq. (6), and b denotes the bias. ω and b indicate the training parameters of the neural network. Finally, we obtain an output convolutional neural network. The form of the loss function is consistent with the RMS deviation (σ).

$$\mathrm{Loss} = \left[\sum_{i=1}^{m} \left(R_{\mathrm{c}}^{\mathrm{Exp.}} - R_{\mathrm{c}}^{\mathrm{Cal.}}\right)^2 \Big/ m\right]^{1/2}, \tag{12}$$

where $R_{\mathrm{c}}^{\mathrm{Cal.}}$ and $R_{\mathrm{c}}^{\mathrm{Exp.}}$ denote the neural network predictions and experimental values of the dataset, respectively, and m indicates the number of dataset.

3 Results and discussions

Based on local CR relations, we propose a neural network containing convolutional layers to study nuclear charge radii. We aimed to explore whether local CR relations could describe the global nuclear charge radii and their ability to predict the charge radii of unknown nuclei.

In this study, datasets were obtained from CR2013 and CR2021 [13, 14]. To test the predictive ability of the neural networks, we selected 814 charge radii data points with $Z \geq 20$ from CR2013 as the training set and 114 charge radii data points from CR2021 as the validation set. The entire set included the training and validation sets, which contained 928 nuclear charge radii.

Similar to alternative neural networks [40, 41, 45], we considered the proton number Z, neutron number N, and mass number A as inputs for the neural network. Owing to the local connection property of the convolutional layer, we must generate the nuclear charge radius data through the fully connected layer and arrange them into a matrix of 79 rows and 153 columns. Here, 79 represents the number of protons, ranging from 18 to 96, and 153 represents the number of neutrons, ranging from 0 to 152. When the loss value of the validation set diminishes to minimum, the generalization of the neural network is optimal. Therefore, we compute the RMS deviation of the entire set for the CNN. The root mean square (RMS) deviations for Eq. (8) and CNN for the training, validation, and entire sets are presented in Table 1. The CNN yielded an RMS deviation of 0.0195 fm for the entire dataset and 0.0156 fm for the validation dataset. Compared to Eq. (8), the entire set is improved by 48% and the accuracy of the validation set significantly improved by 53%.

Subsequently, we provide the radius residuals δR between the experimental $R_{\mathrm{c}}^{\mathrm{Exp.}}$ and the CNN predictions $R_{\mathrm{c}}^{\mathrm{Cal.}}$, i.e.,

$$\delta R = R_{\mathrm{c}}^{\mathrm{Exp.}} - R_{\mathrm{c}}^{\mathrm{Cal.}}. \tag{13}$$

The radius residuals δR of 928 nuclei with proton number Z are denoted in Fig. 3. As observed, $|\delta R| \leq 0.04$ fm for the validation set. $|\delta R| \geq 0.06$ fm for certain heavy nuclei in the training set, especially near the isotopes of $Z = 65$ and 80. In Ref. [59], Fig. 1 displays the significant radii differences for isotopes near $N = 60$, 90, and $Z = 80$. Near the $N = 60$ and 90 regions, the enlarged amplitudes of the radii differences are attributed to the heavy nucleus with a strong static deformation [60–62]. The abnormal radius difference in the $Z = 80$ region is owing to shape staggering, indicating that the shape of the heavy nuclei changes from prolate to oblate, and thereafter, back to prolate [59, 63, 64].

The RMS radii for calcium isotopes from the CNN, Eq. (7), Eq. (8), and experimental data are comparatively presented in Fig. 4a. The experimental data revealed a significant odd–even staggering in the charge radius of the calcium isotopes between $N = 20$ and $N = 28$, with a pronounced shell effect at $N = 28$. Although Eq. (8) contains the δ term, it fails to provide a satisfactory description of the experimental data. In addition, the amplitudes of the odd–even staggering calculated by the CNN were smaller than those of the experimental data. Furthermore, CNN calculations indicate an inverted parabolic trend between $N = 20$ and $N = 28$ along the calcium isotopic chain [5, 65, 66]. The current predictions for the radii of ^{38,49,51}Ca isotopes yielded results were aligned with the available experimental data. The results indicate that the CNN is reliable and provides predictive ability. However, the shell kinks at $N = 20$ and $N =$

Table 1 RMS deviation of training set, validation set, and entire set for Eq. (8) and the proposed neural network (CNN)

	Training set	Validation set	Entire set
$\sigma^{\mathrm{Eq.(8)}}$	0.0384	0.0332	0.0378
σ^{CNN}	0.0201	0.0156	0.0195
$\frac{\sigma^{\mathrm{Eq.(8)}} - \sigma^{\mathrm{CNN}}}{\sigma^{\mathrm{Eq.(8)}}}$	0.48	0.53	0.48

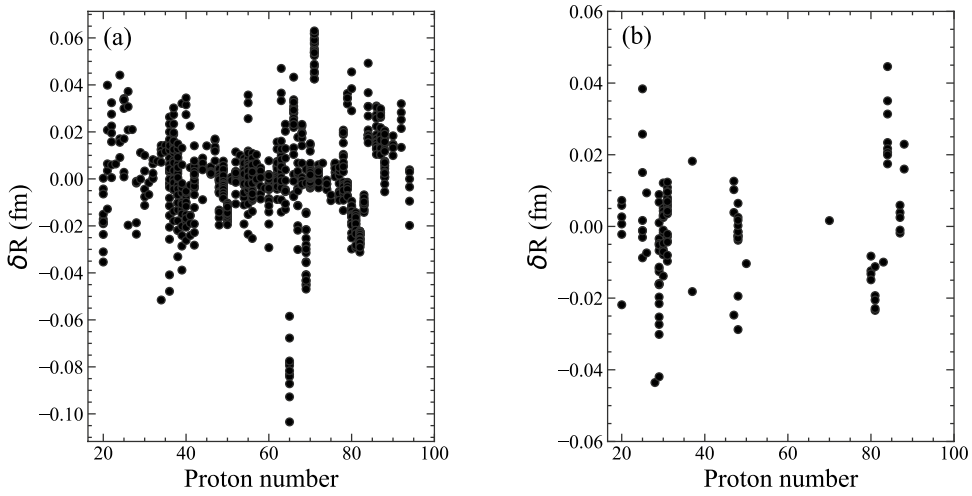

Fig. 3 (Color online) Charge radii residuals $\delta R = R_c^{\text{Exp.}} - R_c^{\text{Cal.}}$ between experimental data and CNN of training set (**a**) and validation set (**b**)

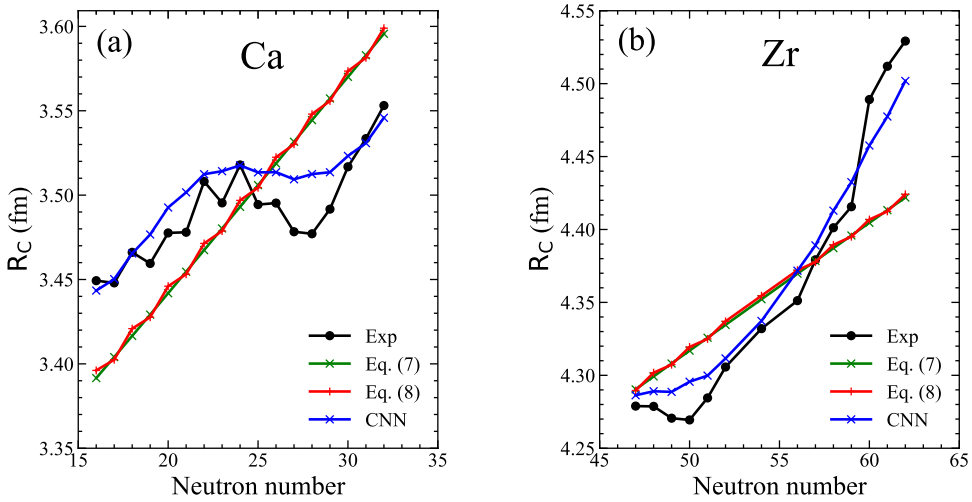

Fig. 4 (Color online) Charge radii of **a** calcium and **b** zirconium isotopes predicted by Eqs. (7), Eq. (8), and CNN, compared with the experimental data

28, as demonstrated by the CNN, were insignificant. Certain studies have employed the macroscopic–microscopic method, incorporating shell corrections and quadrupole and hexadecapole deformations to achieve shell kinks of calcium isotopic chains [5, 65]. As depicted in Fig. 4b, CNN fails to accurately reproduce the prominent shell kinks of zirconium isotopes at $N = 50$, suggesting that accounting for the shell effect may improve the description of nuclear charge radii.

In Ref. [25], a five-parameter formula was proposed that included many physical features such as the shell effect and odd–even staggering. The RMS deviation of the charge radius for nuclei with $A \geq 40$ was 0.023 fm. Recently, Ref. [45] has combined the pairing and shell effects using a three-parameter formula and BNN to describe the nuclear charge radius. The RMS deviation is 0.015 fm for the entire set. In Ref. [51], the inputs of BNN with four engineered features, namely the pairing effect, shell effect, isospin effect, and "abnormal," shape staggering effect. The proposed method obtained an RMS deviation of 0.014 fm for the training and validation datasets. The BNN outperformed the CNN for describing the trend of the nuclear charge radius, indicating that the shell and shape staggering effects can considerably describe the trend of the nuclear charge radius [5, 58].

The difference between the theoretical results of the CNN and the experimental data for all the CR in the entire set is shown in Fig. 5. As observed, the residual of the charge radius of the nucleus located near the shell is less than 0.04 fm, implying that the neural network combined with local CR relations can accurately describe the nuclear charge radius.

4 Summary

We developed a neural network with a convolutional layer to analyze the nuclear charge radii of 928 nuclei. We incorporated the isospin dependence T and pairing relations δ into the convolutional layer to account for the physical

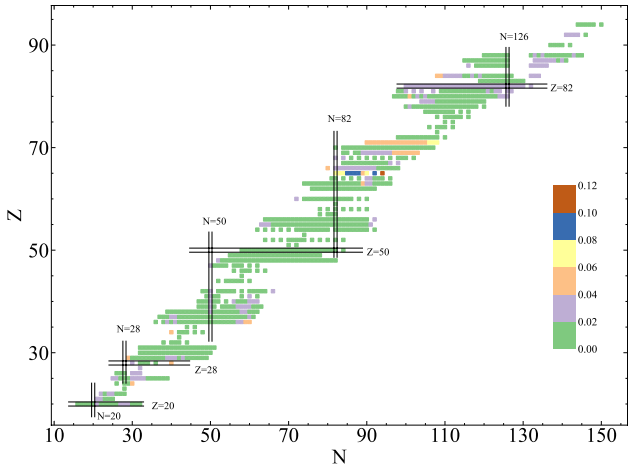

Fig. 5 (Color online) Differences between predicted and experimental values of charge radii for 928 nuclei

factors that influence the nuclear charge radius. The network model achieved an RMS deviation of 0.0201 fm for nuclei with $A \geq 39$ and $Z \geq 20$ in the CR2013 database, and 0.0156 fm for CR2021 as the validation set. The proposed neural network reproduced the trend of the nuclear charge radius, especially the shell effect and odd–even staggerings in calcium isotopes.

There are limitations to the application of convolutional neural networks in terms of the charge radii of the nuclei. Existing experimental data on the nuclear charge radius are limited and scattered. Therefore, we generated data in fully connected layers, such that the regular convolutional kernel in the convolutional layer acted on the data. Presently, the graph convolutional neural networks and deformable convolutional kernels have offered significant advantages in processing irregular data. Perhaps the graph convolutional neural networks can be used to overcome the limitations of the nuclear charge radius data.

Author contributions All authors contributed to the study conception and design. Material preparation, data collection and analysis were performed by Ying-Yu Cao, Jian-You Guo and Bo Zhou. The first draft of the manuscript was written by Ying-Yu Cao and all authors commented on previous versions of the manuscript. All authors read and approved the final manuscript.

Data availability The data that support the findings of this study are openly available in Science Data Bank at https://www.doi.org/10.57760/sciencedb.j00186.00238 and https://cstr.cn/31253.11.sciencedb.j00186.00238.

Declarations

Bo Zhou is an editorial board member for Nuclear Science and Techniques and was not involved in the editorial review, or the decision to publish this article.

Conflict of interests All authors declare that there are no competing interests.

References

1. A. Bohr, B.R. Mottelson, *Nuclear Structure*, vol. One Benjamin, New York (1969). https://doi.org/10.1063/1.3022342
2. H. Limura, F. Buchinger, Charge radii in macroscopic microscopic mass models of reflection asymmetry. Phys. Rev. C **78**, 067301 (2008). https://doi.org/10.1103/PhysRevC.78.067301
3. S. Geldhof, M. Kortelainen, O. Beliuskina et al., Impact of nuclear deformation and pairing on the charge radii of palladium isotopes Phys. Rev. Lett. **128**, 152501 (2022). https://doi.org/10.1103/PhysRevLett.128.152501
4. L.B. Wang, P. Mueller, K. Bailey et al., Laser spectroscopic determination of the ^{6}He nuclear charge radius. Phys. Rev. Lett. **93**, 142501 (2004). https://doi.org/10.1103/PhysRevLett.93.142501
5. N. Wang, T. Li, Shell and isospin effects in nuclear charge radii. Phys. Rev. C **88**, 011301 (2013). https://doi.org/10.1103/PhysRevC.88.011301
6. T.Q. Liang, J. Liu, Z.Z. Ren et al., Elastic electron scattering form factors of deformed exotic Xe isotopes. Phys. Rev. C **98**, 044310 (2018). https://doi.org/10.1103/PhysRevC.98.044310
7. H. De Vries, C.W. De Jager, C. De Vries, Nuclear charge-density-distribution parameters from elastic electron scattering. At. Data Nucl. Data Tables **36**, 495 (1987). https://doi.org/10.1016/0092-640X(87)90013-1
8. K. Heilig, A. Steudel, Changes in mean-square nuclear charge radii from optical isotope shifts. At. Data Nucl. Data Tables **14**, 613 (1974). https://doi.org/10.1016/S0092-640X(74)80006-9
9. P. Aufmuth, K. Heilig, A. Steudel, Changes in mean-square nuclear charge radii from optical isotope shifts. At. Data Nucl. Data Tables **37**, 455 (1987). https://doi.org/10.1016/0092-640X(87)90028-3
10. R. Engfer, H. Schneuwly, J.L. Vuileumier et al., Charge-distribution parameters, isotope shifts, isomer shifts, and magnetic hyperfine constants from muonic atoms. At. Data Nucl. Data Tables **14**, 509 (1974). https://doi.org/10.1016/S0092-640X(74)80003-3
11. G. Fricke, C. Bernhardt, K. Heilig et al., Nuclear ground state charge radii from electromagnetic interactions. At. Data Nucl. Data Tables **60**, 177 (1995). https://doi.org/10.1006/adnd.1995.1007
12. E. Boehm, P.L. Lee, Changes of mean-square nuclear charge radii from isotope shifts of electronic K_{α} X-rays. At. Data Nucl. Data Tables **14**, 605 (1974). https://doi.org/10.1016/S0092-640X(74)80005-7
13. I. Angeli, K.P. Marinova, Table of experimental nuclear ground state charge radii: an update. At. Data Nucl. Data Tables **99**, 69 (2013). https://doi.org/10.1016/j.adt.2011.12.006
14. T. Li, Y. Luo, N. Wang, Compilation of recent nuclear ground state charge radius measurements and tests for models. At. Data Nucl. Data Tables **140**, 101440 (2021). https://doi.org/10.1016/j.adt.2021.101440
15. S. Goriely, S. Hilaire, M. Girod et al., First Gogny–Hartree–Fock–Bogoliubov nuclear mass model. Phys. Rev. Lett. **102**, 242501 (2009). https://doi.org/10.1103/PhysRevLett.102.242501
16. S. Goriely, N. Chamel, J.M. Pearson, Further explorations of Skyrme–Hartree–Fock–Bogoliubov mass formulas. XII. Stiffness and stability of neutron-star matter. Phys. Rev. C **82**, 035804 (2009). https://doi.org/10.1103/PhysRevC.82.035804
17. L.S. Geng, H. Toki, S. Sugimoto et al., Relativistic mean field theory for deformed nuclei with pairing correlations. Prog. Theor. Phys. **110**, 921 (2003). https://doi.org/10.1143/PTP.110.921

18. P.W. Zhao, Z.P. Li, J.M. Yao et al., New parametrization for the nuclear covariant energy density functional with a point-coupling interaction. Phys. Rev. C **82**, 054319 (2010). https://doi.org/10.1103/PhysRevC.82.054319
19. Y. Funaki, T. Yamada, H. Horiuchi et al., α-particle condensation in ^{16}O studied with a full four-body orthogonality condition model calculation. Phys. Rev. Lett. **101**, 082502 (2008). https://doi.org/10.1103/PhysRevLett.101.082502
20. S.Q. Zhang, J. Meng, S.G. Zhou et al., Isospin and $Z^{1/3}$-dependence of the nuclear charge radii. Eur. Phys. J. A **13**, 285 (2002). https://doi.org/10.1007/s10050-002-8757-6
21. Y.A. Lei, Z.H. Zhang, J.Y. Zeng, Improved $Z^{1/3}$ law of nuclear charge radius. Commun. Theor. Phys. **51**, 123 (2009). https://doi.org/10.1088/0253-6102/51/1/23
22. B. Nerlo-Pomorska, K. Pomorski, Isospin dependence of nuclear radius. Z. Phys. A **344**, 359 (1993). https://doi.org/10.1007/BF01283190
23. B. Nerlo-Pomorska, K. Pomorski, Simple formula for nuclear charge radius. Z. Phys. A **348**, 169 (1994). https://doi.org/10.1007/BF01291913
24. G. Royer, R. Rousseau, On the liquid drop model mass formulae and charge radii. Eur. Phys. J. A **42**, 541 (2009). https://doi.org/10.1140/epja/i2008-10745-8
25. Z.Q. Sheng, G.W. Fan, J.F. Qian et al., An effective formula for nuclear charge radii. Eur. Phys. J. A **51**, 4 (2015). https://doi.org/10.1140/epja/i2015-15040-1
26. J. Piekarewicz, M. Centelles, X. Roca-Maza et al., Garvey–Kelson relations for nuclear charge radii. Eur. Phys. J. A **46**, 379 (2010). https://doi.org/10.1140/epja/i2010-11051-8
27. B.H. Sun, Y. Lu, J.P. Peng et al., New charge radius relations for atomic nuclei. Phys. Rev. C **90**, 054318 (2014). https://doi.org/10.1103/PhysRevC.90.054318
28. M. Bao, Y.Y. Zong, Y.M. Zhao et al., Local relations of nuclear charge radii. Phys. Rev. C **102**, 014306 (2020). https://doi.org/10.1103/PhysRevC.102.014306
29. Y.G. Ma, Hypernuclei as a laboratory to test hyperon-nucleon interactions. Nucl. Sci. Tech. **34**, 97 (2023). https://doi.org/10.1007/s41365-023-01248-6
30. R. Wang, Y.G. Ma, R. Wada et al., Nuclear liquid–gas phase transition with machine learning. Phys. Rev. Res. **2**, 043202 (2020). https://doi.org/10.1103/PhysRevResearch.2.043202
31. J. Steinheimer, L. Pang, K. Zhou et al., A machine learning study to identify spinodal clumping in high energy nuclear collisions. JHEP **12**, 122 (2019). https://doi.org/10.1007/JHEP12%282019%29122
32. Y.G. Ma, Effects of α-clustering structure on nuclear reaction and relativistic heavy-ion collisions. Nuclear Techniques **46**(8), 080001 (2023). https://doi.org/10.11889/j.0253-3219.2023.hjs.46.080001 (in Chinese)
33. R. Utama, J. Piekarewicz, H.B. Prosper, Nuclear mass predictions for the crustal composition of neutron stars: a Bayesian neural network approach. Phys. Rev. C **93**, 014311 (2016). https://doi.org/10.1103/PhysRevC.93.014311
34. R. Utama, J. Piekarewicz, Refining mass formulas for astrophysical applications: a Bayesian neural network approach. Phys. Rev. C **96**, 044308 (2017). https://doi.org/10.1103/PhysRevC.96.044308
35. Z.M. Niu, H.Z. Liang, B.H. Sun et al., High precision nuclear mass predictions towards a hundred kilo-electron-volt accuracy. Sci. Bull. **63**, 759 (2018). https://doi.org/10.1016/j.scib.2018.05.009
36. W.B. He, Y.G. Ma, L.G. Pang et al., High-energy nuclear physics meets machine learning. Nucl. Sci. Tech. **34**, 88 (2023). https://doi.org/10.1007/s41365-023-01233-z
37. W.B. He, Q.F. Li, Y.G. Ma et al., Machine learning in nuclear physics at low and intermediate energies. Sci. China Phys. Mech. Astron. **66**, 282001 (2023). https://doi.org/10.1007/s11433-023-2116-0
38. J.J. He, W.B. He, Y.G. Ma et al., Machine-learning-based identification for initial clustering structure in relativistic heavy-ion collisions. Phys. Rev. C **104**, 044902 (2021). https://doi.org/10.1103/PhysRevC.104.044902
39. Y.L. Cheng, S.Z. Shi, Y.G. Ma et al., Examination of nucleon distribution with Bayesian imaging for isobar collisions. Phys. Rev. C **107**, 064909 (2023). https://doi.org/10.1103/PhysRevC.107.064909
40. S. Akkoyun, T. Bayram, S.O. Kara et al., An artificial neural network application on nuclear charge radii. J. Phys. G **40**, 055106 (2013). https://doi.org/10.1088/0954-3899/40/5/055106
41. D. Wu, C.L. Bai, H. Sagawa et al., Calculation of nuclear charge radii with a trained feed-forward neural network. Phys. Rev. C **102**, 054323 (2020). https://doi.org/10.1103/PhysRevC.102.054323
42. R. Utama, W.C. Chen, J. Piekarewicz, Nuclear charge radii: density functional theory meets Bayesian neural networks. J. Phys. G **43**, 114002 (2016). https://doi.org/10.1088/0954-3899/43/11/114002
43. Z.M. Niu, H.Z. Liang, B.H. Sun et al., Predictions of nuclear β-decay half-lives with machine learning and their impact on r-process nucleosynthesis. Phys. Rev. C **99**, 064307 (2019). https://doi.org/10.1103/PhysRevC.99.064307
44. L. Neufcourt, Y.C. Cao, W. Nazarewicz et al., Bayesian approach to model-based extrapolation of nuclear observables. Phys. Rev. C **98**, 034318 (2018). https://doi.org/10.1103/PhysRevC.98.034318
45. X.X. Dong, A. Rong, J.X. Lu et al., Novel Bayesian neural network based approach for nuclear charge radii. Phys. Rev. C **105**, 014308 (2022). https://doi.org/10.1103/PhysRevC.105.014308
46. Z.M. Niu, Z.L. Zhu, Y.F. Niu et al., Radial basis function approach in nuclear mass predictions. Phys. Rev. C **88**, 024325 (2013). https://doi.org/10.1103/PhysRevC.88.024325
47. J.S. Zheng, N.Y. Wang, Z.Y. Wang et al., Mass predictions of the relativistic mean-field model with the radial basis function approach. Phys. Rev. C **90**, 014303 (2014). https://doi.org/10.1103/PhysRevC.90.014303
48. Z.P. Gao, Y.J. Wang, H.L. Lü et al., Machine learning the nuclear mass. Nucl. Sci. Tech. **32**, 109 (2021). https://doi.org/10.1007/s41365-021-00956-1
49. N. Wang, M. Liu, Nuclear mass predictions with a radial basis function approach. Phys. Rev. C **84**, 051303(R) (2011). https://doi.org/10.1103/PhysRevC.84.051303
50. T.S. Shang, J. Li, Z.M. Liu, Prediction of nuclear charge density distribution with feedback neural network. Nucl. Sci. Tech. **33**, 153 (2022). https://doi.org/10.1007/s41365-022-01140-9
51. X.X. Dong, A. Rong, J.X. Lu et al., Nuclear charge radii in Bayesian neural networks revisited. Phys. Lett. B **838**, 137726 (2023). https://doi.org/10.1016/j.physletb.2023.137726
52. Y.Y. Li, F. Zhang, J. Su, Improvement of the Bayesian neural network to study the photoneutron yield cross sections. Nucl. Sci. Tech. **33**, 135 (2022). https://doi.org/10.1007/s41365-022-01131-w
53. K. Mills, M. Spanner, I. Tamblyn, Deep learning and the Schrödinger equation. Phys. Rev. A **96**, 042113 (2017). https://doi.org/10.1103/PhysRevA.96.042113
54. K. Ryczko, D.A. Strubbe, I. Tamblyn, Deep learning and density-functional theory. Phys. Rev. A **100**, 022512 (2019). https://doi.org/10.1103/PhysRevA.100.022512
55. G.T. Garvey, I. Kelson, New nuclidic mass relationship. Phys. Rev. Lett. **16**, 197 (1966). https://doi.org/10.1103/PhysRevLett.16.197
56. G.T. Garvey, W.J. Gerace, R.L. Jaffe et al., Set of nuclear-mass relations and a resultant mass table. Rev. Mod. Phys. **41**, S1 (1969). https://doi.org/10.1103/RevModPhys.41.S1

57. Y. LeCun, B. Boser, J.S. Denker et al., Backpropagation applied to handwritten zip code recognition. Neural Comput. **1**, 541 (1989). https://doi.org/10.1162/neco.1989.1.4.541
58. I. Angeli, Effect of valence nucleons on RMS charge radii and surface thickness. J. Phys. G: Nucl. Part. Phys. **17**, 439 (1991). https://doi.org/10.1088/0954-3899/17/4/006
59. R. An, X.X. Dong, L.G. Cao et al., Local variations of charge radii for nuclei with even Z from 84 to 120. Commun. Theor. Phys. **75**, 035301 (2023). https://doi.org/10.1088/1572-9494/acb58b
60. G.A. Lalazissis, M.M. Sharma, P. Ring, Rare-earth nuclei: radii, isotope-shifts and deformation properties in the relativistic mean-field theory. Nucl. Phys. A **597**, 35 (1996). https://doi.org/10.1016/0375-9474(95)00436-X
61. R.F. Casten, Possible unified interpretation of heavy nuclei. Phys. Rev. Lett. **54**, 1991 (1985). https://doi.org/10.1103/PhysRevLett.54.1991
62. T. Togashi, Y. Tsunoda, T. Otsuka et al., Quantum phase transition in the shape of Zr isotopes. Phys. Rev. Lett. **117**, 172502 (2016). https://doi.org/10.1103/PhysRevLett.117.172502
63. B.A. Marsh, T.D. Goodacre, S. Sels et al., Characterization of the shape-staggering effect in mercury nuclei. Nature Phys. **14**, 1163 (2018). https://doi.org/10.1038/s41567-018-0292-8
64. S. Péru, S. Hilaire, S. Goriely et al., Description of magnetic moments within the Gogny Hartree–Fock-Bogolyubov framework: application to Hg isotopes. Phys. Rev. C **104**, 024328 (2021). https://doi.org/10.1103/PhysRevC.104.024328
65. R. An, L.S. Geng, S.S. Zhang, Novel ansatz for charge radii in density functional theories. Phys. Rev. C **102**, 024307 (2020). https://doi.org/10.1103/PhysRevC.102.024307
66. P.G. Reinhard, W. Nazarewicz, Toward a global description of nuclear charge radii: exploring the Fayans energy density functional. Phys. Rev. C **95**, 064328 (2017). https://doi.org/10.1103/PhysRevC.95.064328